Self-Propelled Rods near Surfaces

Jens Elgeti^{(a)1} and Gerhard Gompper^{(b)1}

Institut für Festkörperforschung, Forschungszentrum Jülich, D-52425 Jülich, Germany

PACS 45.50.-j - Dynamics and kinematics of a particle and a system of particles

PACS 05.40.-a - Fluctuation phenomena, random processes, noise, and Brownian motion

Abstract. - We study the behavior of self-propelled nano- and micro-rods in three dimensions, confined between two parallel walls, by simulations and scaling arguments. Our simulations include thermal fluctuations and hydrodynamic interactions, which are both relevant for the dynamical behavior at nano- to micrometer length scales. In order to investigate the importance hydrodynamic interactions, we also perform Brownian-dynamics-like simulations. In both cases, we find that self-propelled rods display a strong surface excess in confined geometries. An analogy with semi-flexible polymers is employed to derive scaling laws for the dependence on the wall distance, the rod length, and the propulsive force. The simulation data confirm the scaling predictions.

JENS ELGETI^{(a)1} AND GERHARD GOMPPER^{(b)1}

PACS 82.70.-y - Disperse systems; complex fluids
PACS 45.50.-j - Dynamics and kinematics of a particle pack of 5.40.-a - Fluctuation phenomena, random property packs 89.75.Da - Systems obeying scaling laws

Abstract. - We study the behavior of self-propelled confined between two parallel walls, by simulations and thermal fluctuations and hydrodynamic interactions, behavior at nano- to micrometer length scales. In or namic interactions, we also perform Brownian-dynamic interactions, we also perform Brownian-dynamic semi-flexible polymers is employed to derive scaling lather rod length, and the propulsive force. The simulation ogy, there are numerous examples of swimmers and self-propelled particles. With a typical size in the range of a few nano- to several micro-meters, both low-Reynolds-number hydrodynamics [1] and thermal fluctuations are essential to determine their dynamics. Well-known biological examples are sperm cells which are propelled by essential to determine their dynamics. Well-known bioological examples are sperm cells which are propelled by a snake-like motion of their tail [2], bacteria like E. coli which move forward by a rotational motion of their spiral-shaped flagella [3], and listeria which are propelled by local actin polymerization at their surface [4,5]. In soft matter systems, synthetic self-propelled particles have been designed to perform directed motion. Examples are bimetallic nanorods which are driven by different chemical reactions at the two types of surfaces [6–8], or connected chains of magnetic colloidal particles on which a snake-like motion is imposed by an external magnetic field [9].

Both in soft matter and in biological systems, surfaces and walls are ubiquitous. For example, bacteria in wet soil, near surfaces or in microfluidic devices [10, 11], or sperm in the female reproductive tract find themselves in strongly confined geometries. Already in 1963, Rothschild found that sperm accumulate at surfaces [12]. Thus surfaces strongly affect the dynamics of swimmers and selfpropelled particles. Typically, these particles live in an aqueous environment. Therefore, hydrodynamics plays an important role in determining their behavior. The longrange hydrodynamic interactions (at distances from the wall much larger than the particle size, so that the particle can be approximated by a force dipole) induce a parallel orientation and effective attraction to the wall [13,14]. At short distances from the wall, the details of the propulsion mechanism become relevant. For example, it has been shown for E. coli that corkscrew motion of the flagella leads to hydrodynamic attraction [15].

We study here the dynamics of self-propelled rod-like particles confined between two planar walls. Such particles capture the elongated geometry of most of the swimmers mentioned above. In the vicinity of a wall, the rod-like geometry of the particles is important, since it favors parallel orientation — both with and without hydrodynamic interactions. We consider rods which are small enough for thermal fluctuations to play an important role. Thermal fluctuations induce a persistent-random-walk behavior of the trajectories in the bulk, and an entropic repulsion near the wall.

In order to study these effects, we employ a particlebased mesoscale hydrodynamics technique, in which hydrodynamic interactions (HI) can be switched on and off easily. In the absence of hydrodynamic interactions, the effect of the fluid on the self-propelled particle corresponds to a Stokes friction and thermal fluctuations, as described by Brownian dynamics (BD). Our main result is that selfpropelled rods accumulate at surfaces, both with Brownian dynamics and full hydrodynamics. Note that this

⁽a) e-mail:j.elgeti@fz-juelich.de

⁽b)e-mail:g.gompper@fz-juelich.de

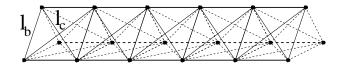


Figure 1: A rod is modeled by three filaments, interconnected by harmonic springs with spring lengths l_b and $l_c = \sqrt{2}l_b$.

result is in contrast to rods pulled parallel to a surface by an external force [16,17]. The aggregation of self-propelled rods is found to depend on the rod length and on the strength of the propulsive force. We employ an analogy with semi-flexible polymers to derive scaling laws for the residence times near and far from the wall, and to distinguish different dynamical regimes.

Model and Simulation Technique. — We model the rod of length l as a crane-like structure (see Fig. 1) [18]. Three semi-flexible filaments, each consisting of N_m monomers, are arranged in a triangular cross section. The distances between the filaments and between monomers within a filament are the same bond length l_b , so that $l = (N_m - 1)l_b$. The rod length is kept nearly constant by harmonic potentials $U_b = K(|\mathbf{r}_{i,i+1}| - l_b)^2$ for the bond vectors $\mathbf{r}_{i,i+1}$ between neighboring monomers, and similarly for next-nearest neighbors. Spring constants Kl_b^2 are chosen to be much larger than the thermal energy $k_B T$, so that length and bending fluctuations are irrelevant.

To describe hydrodynamic behavior, we employ multiparticle collision dynamics (MPC), a particle-based mesoscopic simulation technique that naturally incorporates both hydrodynamic interactions and thermal fluctuations [19-22]. The MPC fluid consists of point-like fluid particles of mass m in continuous space. The dynamics evolves in two steps. During the streaming step, particles propagate ballistically for a time interval h. In the collision step the particles are sorted into the cells of a cubic lattice with cell size a; they exchange momentum by a rotation of their velocities relative to the center-of-mass velocity \mathbf{v}_{cm} of each cell by an angle α around a randomly chosen coordinate axis. We employ the parameters m = 1, $k_BT = 1$, a = 1, h = 0.05, $\alpha = 130^{\circ}$, and $\rho a^3 = 10$ fluid particles per cell. This corresponds to measuring length and time in units of the cell size a and $(ma^2/k_BT)^{1/2}$, respectively. Embedded particles can easily be coupled to the MPC fluid through inclusion of the monomers in the collision step. The crane-like structure of Fig. 1 with bond length $l_b = 0.5a$ and monomer mass M = 5m embedded in a MPC fluid represents a good approximation to slender rods in a Stokes fluid with an effective hydrodynamic radius of r = 0.45a [18]. With the fluid parameters given above, the viscosity is $\eta \simeq 17\sqrt{mk_BT}/a^2$. This is large enough to keep the Reynolds number $Re \equiv \rho l v / \eta < 0.3$ for all considered rod lengths l and rod velocities v.

An advantage of MPC is that hydrodynamic interactions can easily be switched off, while retaining similar thermal fluctuations and friction constants [23,24]. In this

case, denoted random MPC, v_{cm} is drawn from a Maxwell-Boltzmann distribution of variance k_BT/ρ , see Ref. [24]. This allows us to separate Brownian dynamic from hydrodynamic effects.

Propulsion is achieved by applying a forward thrust

$$\mathbf{F}_i = f_t \hat{\mathbf{r}}_{i,i-1} \quad \text{for } i > 1, \tag{1}$$

on each monomer i of the rod, where $\hat{\mathbf{r}}_{i,i-1}$ is the unit vector connecting monomers i and i-1, and f_t is the force strength per monomer. When hydrodynamics is included, an appropriate reaction force is added to the fluid particles in the collision cells occupied by monomers, such that the total momentum is conserved locally. This is equivalent to a rod that pushes the fluid at its surface towards its rear end. We employ a global thermostat to keep the temperature constant. For Brownian dynamics, the velocity v of the rod is proportional to f_t . For our choice of parameters, random MPC gives $|v| \simeq f_t/\gamma_0$ with monomer friction coefficient $\gamma_0 \simeq 270 \sqrt{mk_B T/a^2}$. This leads to the Peclet number

$$Pe = \frac{lv}{D} = \frac{6l^2 f_t}{k_B T},\tag{2}$$

with diffusion constant $D = k_B T/(6\gamma_0 l)$. For $Pe \gg 1$, propulsion dominates and the rod should have a persistent directed motion, while for $Pe \ll 1$ thermal noise dominates and leads to a diffusive behavior.

The rods motion is confined by two parallel hard walls a distance d apart. In the MPC simulations with hydrodynamics, no-slip boundary conditions on the walls are implemented by a bounce-back rule (inversion of the velocity at the wall) and virtual wall particles [21]. In the directions parallel to the walls, we apply periodic boundary conditions. For random MPC, the bounce-back rule is applied to the monomers which hit the wall.

Results. — The main result of our simulations is that self-propelled rods accumulate at a wall, both with and without hydrodynamic interactions, in contrast to passive rods which are depleted near a wall due to entropic reasons. We begin our study with the Brownian-dynamics-type random MPC. The rod accumulation at a wall is illustrated in Fig. 2, which shows the probability density P(z) to find the center of mass of a rod at distance z from the wall for various propulsive forces f_t . Passive rods show a depletion layer of thickness l/2; however, with increasing propulsion force f_t , a pronounced peak develops near the wall. Note that this behavior emerges solely from self-propulsion – i.e. even without hydrodynamic interactions.

 $Surface\ Excess.$ To quantify the surface localization, we define the surface excess

$$s = \int_0^{d/2} \left[P(z) - P_b \right] \mathrm{d}z \tag{3}$$

where P_b is the bulk probability density. A homogeneous distribution corresponds to s = 0, while full absorption at the wall corresponds to s = 1. For a passive rod, P(z)

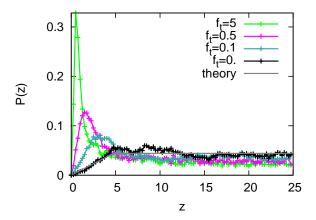


Figure 2: (Color online) Probability density P(z) as function of the distance z from the surface, for various propelling forces f_t . Simulations are performed with Brownian-dynamics-like random MPC. The corresponding surfaces excesses are s=-0.11, s=0.07, s=0.21, and s=0.33 for increasing f_t . The rod length is l=9.5a, the walls are located at z=0a and z=50a. A solid gray line shows the density profile of passive rods.

increases linearly for 0 < z < l/2, and s = -1/(2d/l - 1). To calculate the surface excess in the simulations, we determine the probability $p = \int_0^{l/2} P(z) \mathrm{d}z$ to find the center of mass of the rod within half the rod length from a wall. This can easily be converted into the surface excess via

$$s = (dp - l)/(d - l) \tag{4}$$

with the assumption $P_b = \langle P(z) \rangle_{l/2 < z < d/2}$, which is a good approximation since P(z) is nearly constant for l/2 < z < d/2, see Fig. 2. The surface excess is shown in Fig. 3 as a function of the rod length l for various propulsive forces f_t . Passive rods with $f_t = 0$ show the expected negative surface excess due to entropic repulsion, in good agreement with the analytical equilibrium result. Long propelled rods show a strong surface excess, which decreases for smaller rod lengths (l/a < 10). Short and weakly-propelled rods behave like passive rods (with negative s), but with increasing length, they show a crossover to a positive surface excess, with a minimum of the surface excess at intermediate rod lengths. This minimum occurs at a Peclet number $Pe \simeq 10$. It should be noticed, however, that the dependence of the surface excess on the rod-length l and the propulsive force can *not* be combined into a dependence on the Peclet number alone — for example, because the curves for large f_t in Fig. 3 depend on l but are essentially independent of f_t .

Scaling Arguments. In order to understand the mechanism which is responsible for the effective surface adhesion of self-propelled rods, and to predict their behavior as a function of rod length, propulsive force, and wall separation, we exploit the analogy of the trajectories of self-propelled rods with the conformations of semi-flexible polymers. In the bulk, the rotational diffusion constant

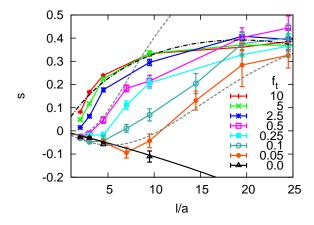


Figure 3: (Color online) Surface excess s as a function of scaled rod length l/a, for various propelling forces f_t , as indicated. Simulations are performed with Brownian-dynamics-like random MPC. The (black) dashed-dotted line is the scaling result in the ballistic regime (see Eq. (8)), the (gray) dashed lines are scaling results in the diffusive regime (see Eq. (10)) for $f_t = 0.5$ and $f_t = 0.05$. Wall distance is d = 50a.

of a rod is $D_r \sim k_B T/(\eta l^3)$, which implies a persistence length

$$\xi_p \sim v/D_r \sim \eta v l^3/k_B T$$
 (5)

of the trajectory. The probability to find the self-propelled rod in a layer of thickness l/2 near the wall can be expressed as $p = \tau_w/(\tau_w + \tau_b)$, where τ_w is the time the rod remains within this layer and τ_b is the time it is located in the bulk (with l/2 < z < d - l/2). The surface excess is then obtained from Eq. (4).

To estimate τ_w , we consider a rod, which at time t=0 is oriented parallel to the wall, and located very close to the wall with $0 < z \ll l/2$. As the rod moves forward, it is reflected when is hits the wall, and is thereby constrained to the positive half-space z>0, see Fig. 4. This situation is very similar to a semi-flexible polymer, which is fixed at one end near the wall with tangent vector parallel to the wall; its bending rigidity κ is determined by the persistence length, $\xi_p = \kappa/k_B T$. In this case, the distance of the polymers from the wall increases as $\langle z \rangle \sim (k_B T/\kappa)^{1/2} x^{3/2}$ and the orientation angle as $\langle \theta \rangle \sim (k_B T/\kappa)^{1/2} x^{1/2}$, where x=vt is the distance traveled parallel to the wall [25, 26]. The condition $\langle z \rangle = l/2$ at $t=\tau_w$ then implies

$$\tau_w \sim \frac{1}{v} \left(l^2 \xi_p \right)^{1/3} \sim \left(\frac{\eta}{k_B T} \right)^{1/3} l^{5/3} v^{-2/3}.$$
 (6)

It is important to emphasize that there is no complete analogy between semi-flexible polymers and self-propelled rods. The main difference is that the equilibrium conformations of long semi-flexible polymers touch a wall essentially tangentially – with a very small angle on both sides determined by the bending rigidity. The trajectory of a self-propelled rod, on the other hand, can approach a wall also almost perpendicularly, see Fig. 4. The rod will hit the wall and get stuck at first, but under the effect

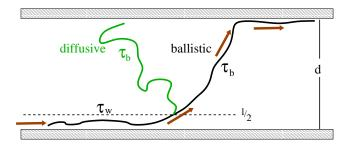


Figure 4: (Color online) Schematic representation of the different regimes of rod motion, near a wall for time τ_w , and in the bulk for time τ_b , either in the ballistic or in the diffusive regime.

of a small wall slip and thermal fluctuations, it will then slowly reorient itself parallel to the wall. Thus, it should be noticed that we employ the polymer analogy only for those parts of the trajectory at the wall after the rod has oriented itself parallel to the wall.

For the time τ_b for the rod to stay in the bulk fluid, we have to distinguish two regimes. In the ballistic regime, with $\xi_p \gg d$, the rod travels essentially on a straight line between the walls, see Fig. 4. In this case, the bulk time is given by $\tau_b \sim v^{-1}d/\sin(\theta)$, where θ is the angle of the rod with the surface when it leaves the wall layer of thickness l/2. The polymer analogy explained above implies $\langle \theta \rangle \sim (l/\xi_p)^{1/3}$ for $\theta \ll 1$, so that

$$\tau_b \sim \frac{d}{v} \left(\frac{\xi_p}{l}\right)^{1/3} \sim \left(\frac{\eta}{k_B T}\right)^{1/3} d \, l^{2/3} \, v^{-2/3}.$$
 (7)

Thus, the scaling arguments predict in the ballistic regime the probability

$$p = l/(l + a_B d) \tag{8}$$

to find the rod in the wall layers, with a constant a_B which has to be determined numerically. Note that this expression is independent of the velocity v, because both time scales τ_w and τ_b depend on v in the same way.

In the diffusive regime, the persistence length ξ_p is small compared to the slit width d. In this case, the calculation of τ_b is a mean first-passage time problem [27]. The mean first-passage time for a one-dimensional random walker starting at position z_0 to reach one of the walls is $\tau_1 \sim z_0(d-z_0)\,\tau_0/\xi_p^2$, with the time unit $\tau_0 \sim \xi_p/v$. For $z_0 \ll d$, this implies $\tau_b \sim z_0 d$. We take $z_0 \sim \xi_p \sin(\theta)$, because this is the distance from the wall layer which the rod travels before it forgets its orientation, and obtain

$$\tau_b \sim \frac{d}{v} \left(\frac{l}{\xi_p}\right)^{1/3} \sim \left(\frac{\eta}{k_B T}\right)^{-1/3} d \, l^{-2/3} \, v^{-4/3}.$$
 (9)

Thus, in the diffusive regime, the scaling arguments imply

$$p = \frac{l}{l + a_D d f_t^{-2/3} l^{-4/3}}$$
 (10)

with a constant a_D , where we have used that $v \sim f_t$. Although p depends on f_t (or v) in this case, this dependence decreases with increasing rod length l.

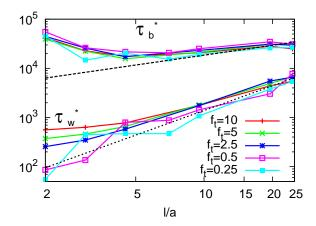


Figure 5: (Color online) Rescaled wall time $\tau_w^* = \tau_w f_t^{2/3}$ and bulk time $\tau_b^* = \tau_b f_t^{2/3}/10$ for different propulsive forces f_t , as indicated. Dashed lines are scaling predictions $\tau_w \sim l^{5/3}$ and $\tau_b \sim l^{2/3}$. The wall separation is d = 50a.

In order to test our scaling predictions, we show in Fig. 5 the scaled times $\tau_w f_t^{2/3}$ and $\tau_b f_t^{2/3}$, as determined from the simulations. For sufficiently long rods, $l \gtrsim 5a$, and not too small forces, $f_t \gtrsim 0.5$, the simulation results are found to agree very well with the scaling predictions (6), (7). We have also investigated numerically the d-dependence of τ_b in the diffusive regime, and find good agreement with the linear dependence predicted by Eq. (9).

The scaling results (8), (10) can now be used together with Eq. (4) to determine the surface excess s. With a single set of numerical prefactors $a_B = 0.23$ and $a_D = 2.48$, the l-dependence in Fig. 3 can be described very well for various propulsion forces f_t . This allows for the following interpretation. Simulations with strong propulsion, $f_t > 2.5$, are in the ballistic regime. With weaker propulsion, short rods are in the diffusive regime. With increasing rod length, the persistence length of the trajectory $(\xi_p \sim vl^3)$ increases, leading to a crossover to the ballistic regime. For long rods, l > 20a, this leads to a surface excess independent of f_t over more than two orders of magnitude, in excellent agreement with Eq. (8).

Fig. 6 shows the dependence of the surface excess on the propulsive force f_t in more detail. For small f_t , the surface excess equals that of a passive rod. The surface excess increases, when the propulsive force becomes relevant compared to the thermal motion; it reaches a plateau when the persistence length becomes comparable to the wall separation d. These simulations results are again in good agreement with the scaling predictions.

Hydrodynamic Interactions. In order to assess the effect of hydrodynamic interactions, we compare in Figs. 6 and 7 results of simulations with Brownian-type dynamics (BD) and full hydrodynamics. We focus here on rod lengths $l \leq 10a$ in order to obtain good statistical accuracy. The simulations show that the qualitative behavior is very similar as without hydrodynamic interactions.

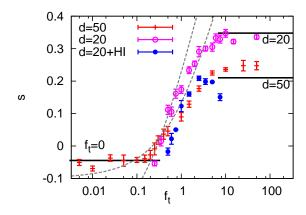


Figure 6: (Color online) Surface excess s as a function of propulsive force f_t . The parameters are $l=4.5\,a$, and $d=20\,a$ or $d=50\,a$ as indicated. The solid lines show the predicted asymptotic behaviors for small and large propulsive forces. The dashed lines indicate the scaling results in the diffusive regime (see Eq. (10)). The decrease of s for $f_t \simeq 4$ with HI is probably a finite-Reynold-number effect ($Re \simeq 0.3$).

However, hydrodynamic interactions *reduce* the surface excess. This effect is most pronounced for intermediate rod lengths, see Fig. 7, and persists over a wide parameter range.

For a rod moving far from a wall, hydrodynamic interactions increase the rotational diffusion coefficient and decrease the translational friction coefficient logarithmically as a function of the rod length [28],

$$D_r = \frac{3k_B T}{\pi \eta l^3} \left[\ln(l/2r) - 0.66 + \mathcal{O}(r/l) \right] , \quad (11)$$

$$\gamma_{\parallel} = 2\pi \eta l \left[\ln(l/2r) - 0.21 + \mathcal{O}(r/l) \right]^{-1}, \quad (12)^{-1}$$

where 2r is the rod diameter. Thus a rod with hydrodynamic interactions (HI) should move faster than without at the same propulsion force, as it is indeed seen in our simulations. However, the persistence length of its trajectory, $\xi_p \sim v/D_r \sim f_t/(\gamma_{\parallel}D_r)$, does not change, since the logarithmic factors cancel out (to leading order for long rods). When we insert these results in our scaling relations, we find that both τ_b and τ_w are reduced in the presence of hydrodynamic interactions by a factor $1/\ln(l/2r)$, while the ratio τ_w/τ_b remains unaffected in both the diffusive and the ballistic scaling regimes (to leading order for large l/a.)

Fig. 8 shows our simulation results for the ratio $\tau_w(HI)/\tau_w(BD)$ and $\tau_b(HI)/\tau_b(BD)$ for systems with and without hydrodynamics. Clearly, hydrodynamic interactions speed up both processes. The observed decay with increasing rod length is in good qualitative agreement with the scaling prediction of a logarithmic dependence on the rod-length.

However, the logarithmic factors in τ_w and τ_b cannot explain the smaller surface excess with HI observed in Fig. 7, because s only depends on the ratio τ_w/τ_b . The reason for

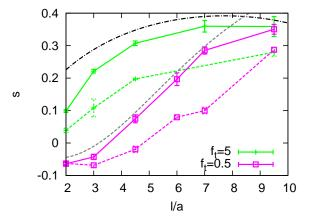


Figure 7: (Color online) Surface excess s as a function of scaled rod length l/a. Symbols show simulation results with (dashed line) and without (solid line) HI for different propulsive forces f_t , as indicated. The dashed-dotted line shows the scaling result in the ballistic regime (see Eq. (8)), the dashed line in the diffusive regime (see Eq. (10)). Wall distance is d = 20a.

the decreased surface excess is that τ_w decreases more than τ_b , see Fig. 8. In order to better understand the behavior of these characteristic times, we show in Fig. 9 the distribution P of τ_w and τ_b for the same intermediate strength of the propulsive force as in Fig. 7. For Brownian-dynamicstype simulations, the distribution shows an initial decay at small τ , followed by a second peak, both in τ_w and τ_b . The two peaks in $P(\tau_b)$ are caused by two different processes after the rod leaves the wall region, (i) reentry to the same wall after a short time under a flat angle, and (ii) crossing of the channel and reaching the other wall under a steeper angle. The same mechanisms are also responsible for the peaks in $P(\tau_w)$, because a steeper entrance angle into the wall layer implies a deeper penetration and thereby a longer residence time in the wall layer. The second peak gets larger when the rod gets longer and crossings are more likely than reentries due to the larger persistence lengths.

For hydrodynamically interacting rods, Fig. 9 shows that the probability for short residence times in the wall and the bulk regions is significantly enhanced. No second peak is visible for rod length l/a=7, but it develops for longer rods with l/a=9.5.

The reason for the stronger decrease of τ_w than τ_b when HI are switched on must be the hydrodynamic interaction with the wall. The far-field approximation of this interaction [13, 14] is certainly not quantitatively correct for the long rods and small wall separations we consider; however, it could still apply qualitatively. For $\theta \ll 1$, it predicts a hydrodynamic torque proportional to $p\theta/z^3$, with dipole moment $p \sim \eta v l^2$, at a distance z from the wall [14]. This implies that as the rod moves towards the wall, it gets oriented parallel to the wall, and therefore penetrates less deeply into the wall layer. The torque can be expressed as an effective orientational potential

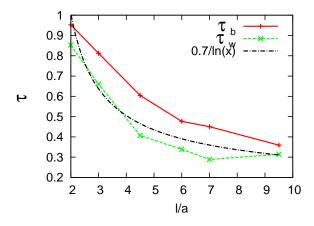


Figure 8: (Color online) Ratios $\tau_w(HI)/\tau_w(BD)$ and $\tau_b(HI)/\tau_b(BD)$ of residence times for simulations with hydrodynamic interaction and Brownian dynamics, as a function of the rod-length l/a. The propulsive force is $f_t = 0.5$, the wall distance is d = 20a. The dashed-dotted line indicates the logarithmic dependence expected from Eqs. (11) and (12).

 $W_r \sim p\theta^2/z^3$. Thus, for small angles $|\theta|$ (and large distances z) where $W_r < k_B T$, orientational diffusion still dominates. The combination of hydrodynamic alignment and small orientational fluctuations is consistent with the increase of short residence times in the distributions of Fig. 9 when hydrodynamic interactions are switched on.

Summary. — We have shown that self-propelled rods in confined geometries show a strong surface excess. The surface excess is negative for a passive rod; it increases with the propulsive force, and saturates for large forces. The analogy with semi-flexible polymers allows the prediction of scaling laws, which are in good agreement with the simulation results. Our results for the aggregation of self-propelled rods at surfaces are relevant for many systems in biology and nanotechnology.

References

- [1] Purcell E. M., Am. J. Phys., 45 (1977) 3.
- [2] Gray J., J. Exp. Biol., **32** (1955) 775.
- [3] Berg H. C., E. coli in Motion (Springer, New York) 2004.
- [4] Bernheim-Groswasser A., Wiesner S., Golsteyn R. M., Carlier M.-F. and Sykes C., *Nature* , 417 (2002) 308.
- [5] BOUKELLAL H., CAMPÁS O., JOANNY J.-F., PROST J. and SYKES C., Phys. Rev. E, 69 (2004) 061906.
- [6] PAXTON W. F., KISTLER K. C., OLMEDA C. C., SEN A., ST. ANGELO S. K., CAO Y., MALLOUK T. E., LAMMERT P. E. and CRESPI V. H., J. Am. Chem. Soc., 126 (2004) 13424.
- [7] FOURNIER-BIDOZ A., ARSENAULT A. C., MANNERS I. and OZIN G. A., Chem. Commun., (2005) 441.
- [8] RÜCKNER G. and KAPRAL R., Phys. Rev. Lett., 98 (2007) 150603.
- [9] DREYFUS R., BAUDRY J., ROPER M. L., FERMIGIER M., STONE H. A. and BIBETTE J., Nature, 437 (2005) 862.

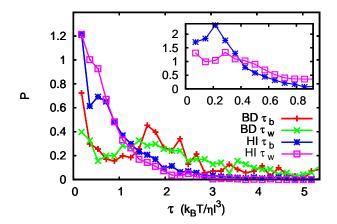


Figure 9: (Color online) Probability distribution of residence times τ_w and τ_b , both for systems with HI and BD. The propulsive force is $f_t = 0.5$, the wall separation d = 20a. Rod lengths are l/a = 7 and l/a = 9.5 (inset).

- [10] DILUZIO W. R., TURNER L., MAYER M., GARSTECKI P., WEIBEL D. B., BERG H. C. and WHITESIDES G. M., Nature, 435 (2005) 1271.
- [11] GALAJDA P., KEYMER J., CHAIKIN P. and AUSTIN R., J. Bacteriol., 189 (2007) 8704.
- [12] Rothschild, Nature, 198 (1963) 1221.
- [13] PEDLEY T. J. and KESSLER J. O., Annu. Rev. Fluid Mech., 24 (1992) 313.
- [14] BERKE A. P., TURNER L., BERG H. C. and LAUGA E., Phys. Rev. Lett., 101 (2008) 038102.
- [15] LAUGA E., DILUZIO W. R., WHITESIDES G. M. and STONE H. A., Biophys. J., 90 (2006) 400.
- [16] RUSSEL W. B., HINCH E. J., LEAL L. G. and TIEFFEN-BRUCK G., J. Fluid Mech., 83 (1977) 273.
- [17] SENDNER C. and NETZ R. R., EPL, 79 (2007) 58004.
- [18] ELGETI J. and GOMPPER G., Hydrodynamics of active mesoscopic systems in NIC Symposium 2008, edited by MÜNSTER G., WOLF D. and KREMER M., Vol. 39 of NIC series (Neumann Institute for Computing, Jülich) 2008 pp. 53-61; http://www.fz-juelich.de/nic-series/volume39/.
- [19] MALEVANETS A. and KAPRAL R., J. Chem. Phys., 110 (1999) 8605.
- [20] IHLE T. and KROLL D. M., Phys. Rev. E , 63 (2001) 020201(R).
- [21] LAMURA A., GOMPPER G., IHLE T. and KROLL D. M., Europhys. Lett., 56 (2001) 319.
- [22] RIPOLL M., MUSSAWISADE K., WINKLER R. G. and GOMPPER G., Europhys. Lett., 68 (2004) 106.
- [23] KIKUCHI N., GENT A. and YEOMANS J. M., Eur. Phys. J. E, 9 (2002) 63.
- [24] RIPOLL M., WINKLER R. G. and GOMPPER G., Eur. Phys. J. E , 23 (2007) 349.
- [25] MAGGS A. C., HUSE D. A. and LEIBLER S., Europhys. Lett., 8 (1989) 615.
- [26] Burkhardt T. W., J. Stat. Mech., (2007) P07004.
- [27] FELLER W., An introduction to probability theory and its applications 3rd Edition Vol. 1 (Wiley, New York) 1968.
- [28] TIRADO M. M. and GARCIA DE LA TORRE J., J. Chem. Phys., 73 (1980) 1986.